

The Gas Dynamics of NGC 4472 Revealed by *XMM-Newton*

R. P. Kraft¹, W. R. Forman¹, C. Jones¹, P. E. J. Nulsen¹, M. J. Hardcastle², S. Raychaudhury³, D. A. Evans⁴, G. R. Sivakoff⁵, C. L. Sarazin⁵

ABSTRACT

We present results from a 100 ks *XMM-Newton* observation of the hot gas in the Virgo cluster elliptical galaxy NGC 4472. We find a surface brightness discontinuity ~ 21 kpc north of the nucleus, consistent with being a contact discontinuity between two moving fluids. We also detect a >60 kpc long ram-pressure stripped tail. The pressure across the discontinuity implies an infall velocity, v_{infall} , of $1000 \text{ km s}^{-1} < v_{\text{infall}} < 2200 \text{ km s}^{-1}$ depending on what assumptions are made about the density and pressure of the external gas. We suggest that the NGC 4472 group is falling into a collapsing filament, which is itself falling into the Virgo cluster. The gas of a collapsing filament is rapidly decelerated as it crosses the standoff shock, but the apparent high velocity of infall of NGC 4472 could be simply due to the fact that the gravitating potential of the NGC 4472 group is unaffected by this shock. The group will fall through the shock its gas will be stripped as it passed through the stalled gas of the filament. Additionally, we find two sets of cool filamentary arms to the east and the southwest of the nucleus. One of the southwest arms is co-incident with a sharp filament seen with *Chandra*. We interpret these arms as filaments of cool gas that have been driven out from the center of the galaxy by the buoyant evolution of a radio bubble. The age of this outburst is $\sim 10^8$ yrs assuming that the buoyant bubble rises with a velocity of $\sim 0.4c_s = 200 \text{ km s}^{-1}$ and the energy of the outburst is a modest $\sim 2 \times 10^{56}$ ergs.

Subject headings: galaxies: individual (NGC 4472) - X-rays: galaxies - hydrodynamics - galaxies: jets

¹Harvard-Smithsonian Center for Astrophysics, 60 Garden St., MS-67, Cambridge, MA 02138

²University of Hertfordshire, School of Physics, Astronomy, and Mathematics, Hatfield AL10 9AB, UK

³University of Birmingham, School of Physics and Astronomy, Edgbaston, Birmingham, B15, 2TT, UK

⁴MIT Kavli Institute for Astrophysics and Space Research, 77 Massachusetts Ave., Cambridge, MA 02139, USA

⁵University of Virginia, Department of Astronomy, Charlottesville, VA 22904, USA

1. Introduction

The *Chandra* and *XMM-Newton* X-ray observatories have profoundly influenced our understanding of gas dynamics in early-type galaxies and clusters of galaxies. The angular resolution and effective area of this pair of observatories permits us to study the gas in these systems from scales of pc for the nearest elliptical galaxies to Mpc (i.e. near the virial radius) for distant, massive clusters. We now routinely measure temperature, density, and metallicity gradients in the hot coronae of these systems which are indicative of a variety of subsonic and supersonic gas motions in the gravitating dark matter potential of these systems. The interplay between the keV baryons and the dark matter of high redshift clusters is of particular importance in determination of cosmological parameters.

XMM-Newton and *Chandra* have shown that feedback between the supermassive black holes of the central dominant galaxies and the hot gas in clusters of galaxies play a critical role in the energy budget of the gas cores and can effectively suppress the formation of cooling flows. Intermittent nuclear outbursts producing radio jets and lobes can occasionally remove or reheat the radiatively cooling gas at the centers of these systems, limiting the amount of gas that will cool from the hot atmosphere and form stars (Churazov *et al.* 2002). Nuclear activity also may play a key role in the suppression of star formation, thus limiting the mass of both the central SMBH and the galaxy (Croton *et al.* 2006). However, the details of the interaction between the nuclear outbursts and the ambient gas are still far from understood. *Chandra* and *XMM-Newton* have observed a wide range of features in the gas of groups and clusters of galaxies related to nuclear outbursts including shocks, cold rims around bubbles, and filamentary structures. In addition to offsetting any radiative cooling at the center, these nuclear outbursts also probably play a key role in mixing the enriched material from the cluster center with the lower abundance gas at larger radii.

Similarly, *XMM-Newton* and *Chandra* observations have revealed a wealth of complex features in the gas which are the result of mergers. Strong shocks have been studied merging pairs of massive clusters, such as the Bullet cluster (Markevitch *et al.* 2002). Study of these shocks can provide important clues about the transport properties of the ICM and on the interaction cross-section of the dark matter (Markevitch *et al.* 2004). Transsonic galaxy or cluster mergers create ram-pressure stripped cores, or cold fronts, such as seen in the Fornax cluster (Machacek *et al.* 2006) and Abell 1367 (Vikhlinin *et al.* 2001). Even less dramatic mergers can create significant disturbances in the gas. The central cores of clusters and galaxies can be displaced from the gravitating dark matter potential by a merger with a sub-halo (or even a close passage) (Markevitch & Vikhlinin 2007), creating the appearance of a surface brightness discontinuity in the gas. Mergers of all sizes almost certainly play an important role in mixing the metals from the central early-type galaxy thrown of in

supernovae and stellar winds with the larger scale primordial gas. These phenomena are all the result of mergers over a wide range of mass scales and energies, and the study of these objects provide us with important clues about the formation of structure.

NGC 4472 (M49) is the dominant member of a group of galaxies that is falling into the Virgo cluster (Tonry *et al.* 2001, $d \sim 16$ Mpc, $1' = 4.65$ kpc), and is one of the most massive (Côté *et al.* 2003, $\sim 8 \times 10^{11} M_{\odot}$) and X-ray luminous early-type galaxies in the local Universe. It is, in fact, the brightest optical galaxy in the Virgo cluster (brighter than M87 by ~ 0.2 magnitudes), but more than an order of magnitude fainter in X-rays than M87. NGC 4472 has a bright ($L_X \sim 10^{42}$ ergs s^{-1}) gaseous corona (Forman *et al.* 1985, 1993), and a long (100 kpc), diffuse ‘tail’, that is believed to be the result of ram-pressure stripping due to infall into the Virgo cluster (Irwin & Sarazin 1996). Based on the pressure jump between the NGC 4472 group gas and the Virgo cluster gas measured with *ROSAT*, Irwin & Sarazin (1996) argue that NGC 4472 is falling into the Virgo cluster supersonically (Mach number > 2) even though it lies at roughly the virial radius. If this is correct, the bow shock should be readily visible in a deep *XMM-Newton* observation. In our first paper on NGC 4472 (Biller *et al.* 2004) we reported the detection of small cavities in the gas coincident with radio lobes within $\sim 2'$ of the nucleus based on a 40 ks ACIS-S observation. We also detected a filamentary tail extending at least 36 kpc south of the nucleus which we attributed to ram-pressure stripping as a result of the infall of the group into the Virgo cluster. Recent *Suzaku* measurements, in combination with the archival *XMM-Newton* data, show a complex spatial dependence of the heavy elements and a depletion of O relative to higher Z metals.

In this paper, we present results from a 100 ks *XMM-Newton* observation of the hot gas in NGC 4472. The large effective area and high count rate facilitate a detailed study of the gas dynamics in this galaxy and the interaction between the NGC 4472 group gas and the larger scale Virgo cluster gas. We also reprocessed and reanalyzed the the publically available archival *Chandra* data. This paper is organized as follows. Section 2 contains a brief summary of the *XMM-Newton* data. Analysis is presented in Section 3, followed by an interpretation of our results in Section 4. Section 5 contains a brief summary and conclusion. We adopt a distance of 16.7 Mpc to NGC 4472 (Blakeslee *et al.* 2009). At this distance, $1'' = 81$ pc and $1' = 4.86$ kpc. All uncertainties are at 90% confidence for one parameter of interest unless otherwise stated, and all coordinates are J2000. All spectral fits include absorption ($N_H = 1.62 \times 10^{20}$ cm^{-2}) by foreground gas in our Galaxy (Dickey & Lockman 1990) using the elemental abundances of Anders & Grevesse (1989) within the *phabs* model of XSPEC12.

2. Data Preparation

NGC 4472 was observed for ~ 100 ks with *XMM-Newton* on January 1, 2004 (OBSID 0200130101, revolution 744) with the Thin filter inserted. The *XMM-Newton* ODF files were reprocessed using SAS version xmmas-20090615-1801-9.0.0 to ensure that the latest calibration products were applied to the event files. The MOS and PN event files were filtered using strict criteria for highest energy resolution. All events in the MOS event files with FLAG>0 and PATTERN>12 were excluded. All events in the PN event file with FLAG>0 and PATTERN>4 were excluded. Light curves were made for all three event files in the 5.0-10.0 keV band and periods when the background exceeded the mean value by more than 3σ were removed. The time removed due to background flaring was relatively small. Flare filtering left 93269 s, 93310 s, and 80445 s of live time in the MOS1, MOS2, and PN cameras, respectively. All point sources visible by eye were excluded from our analysis. Specifically tailored *XMM-Newton* background files were created using data from *XMM-Newton* pointed observations within 25° of NGC 4472 and with Galactic column densities between $1\text{-}3 \times 10^{20}$ cm^{-2} . We also used local background and the nominal dark sky background files. Our results are generally insensitive to which background was used because the diffuse gas is so bright. The out of time events from the bright central core are readily visible in the PN images, so we also corrected all spectra for these events. If not removed, these events would reduce the derived temperatures in the lower surface brightness halo.

An archival *Chandra*/ACIS-S (40 ks, OBSID 321) observation was also used for some analysis presented in this paper. A shorter *Chandra*/ACIS-I observation (10 ks, OBSID 322) was not used because the complexity of handling two backgrounds, two instruments responses, etc., far outweighed the modest gain in exposure. The *Chandra* data were reprocessed using CIAO 4.0, flare filtered, and destreaked using the standard techniques. The livetime remaining after flare filtering was 33960 s.

3. Analysis

An exposure corrected *XMM-Newton* image (MOS1+MOS2 coadded) of the diffuse gas in NGC 4472 in the 0.5-2.0 keV band is shown in Figure 1. The point sources were detected using a wavelet decomposition (the CIAO tool *wavdetect*) and have been removed from the image. The emission from the diffuse gas was estimated in elliptical annuli around the point sources and added back into the image with a random Poisson deviate to give a smooth appearance. The diffuse emission has an elliptical shape with the major axis aligned northeast-southwest (Forman *et al.* 1985, 1993). The diffuse tail, first reported in a ROSAT observation of NGC 4472 (Irwin & Sarazin 1996), can be seen extending to the southwest.

An irregular surface brightness discontinuity lies along the northern boundary of the gas. The portion of this discontinuity directly to the north of the nucleus is coincident with a feature seen in the *Chandra* observation (Biller *et al.* 2004). In this previous paper, we argued that this was the contact discontinuity between the group gas of the NGC 4472 system and the Virgo cluster gas.

The primary scientific goals of this work are to use the imaging and spectroscopic capabilities of the *XMM-Newton* observatory to constrain the large scale gas dynamics of NGC 4472 and search for features related to the merger with the Virgo cluster or evidence of earlier nuclear outbursts. Our analysis proceeds along three lines. We initially created images in different bands and made a temperature map to search for any temperature structures indicative of shocks, cold filaments, and cold fronts that are indicative of gas motions. We then deprojected the spectra from annular bins to determine the temperature, density, and elemental abundance profile in azimuthally symmetric bins. Finally, we created profiles across surface brightness discontinuities in the gas on large (tens of kpc) scales to constrain the dynamics of the merger with the Virgo cluster.

3.1. Temperature Map

Smoothed, exposure corrected images (MOS1+MOS2 co-added) in the 0.5-1.0 keV and 1.0-1.5 keV bands are shown in Figures 2 and 3, respectively. Note the four filamentary arms extending to the east and the southwest of the nucleus in Figure 2. These features are absent in the harder band image (Figure 3) suggesting that they are filaments of cool gas that have been dredged up from the center. The southwest filament is coincident with the filament seen in the *Chandra* observation (Biller *et al.* 2004) and was attributed to the stripping of the NGC 4472 group gas by the infall into the Virgo cluster.

We created a temperature map using the images in the two energy bands shown in Figures 2 and 3. The map was created by determining the count ratio, R , (soft band rate divided by hard band rate) in each pixel after subtraction of a suitable background. Using XSPEC, we computed the ratio for gas temperatures in the range 0.7 keV to 1.5 keV assuming an VAPEC model with abundances of O, Si, S, and Fe determined from the spectral fits described below and Galactic ($N_H=1.62\times 10^{20}$ cm⁻²) absorption. A second order polynomial was fit to the predicted value of R as a function of temperature to create an analytic function to convert R to gas temperature. Variations of this technique are widely used to create temperature maps from *Chandra* data (e.g. David *et al.* 2009, among others) and works well because the centroid of the Fe L complex is a strong function of the gas temperature. The results are insensitive to the assumed abundances since we are

simply mapping the centroid of the Fe L complex to temperature. The limiting systematic uncertainties of this model are a result of the assumptions that the plasma has a single temperature at each point and that the abundances of all the metals scale by a single factor relative to the Solar value.

The temperature map is shown in Figure 5. The approximate positions of the filaments seen in the soft band image (Figure 2) are labeled with the green arrows. The approximate position of the contact discontinuity with the Virgo cluster gas is shown with the white arrows. Several features are apparent from this image. First, the filaments are cooler (~ 0.9 keV) than the surrounding gas (1.15 keV). They are therefore not shocks. Second, there is a cool (~ 0.80 keV) core about $1'$ (5 kpc) in radius at the center of the group. There is a region of cool gas to the southeast of this cool core. The gas to the northwest (i.e. in the direction of M87) is considerably hotter (~ 1.15 keV).

The effect of the kpc-scale temperature variations in the central region of NGC 4472 can be seen more clearly in Figure 6. This figure contains plots of the radial surface brightness profile of the emission in two 40° wedges centered on the nucleus detected in the *Chandra*/ACIS-S observation in the 0.5-2.0 keV band. The vertical lines denote the positions of surface brightness discontinuities in the gas. The stellar light distribution, and therefore the gravitational potential, is fairly smooth, so that these surface brightness discontinuities must either represent contact discontinuities in the gas or (less likely) sound waves similar to those seen in the Perseus cluster (Fabian *et al.* 2003). The temperature jumps across these discontinuities are suggestive of ‘sloshing’ (Markevitch & Vikhlinin 2007). Note the azimuthal asymmetry of these features, which is indicative of complex gas motions. The existing *Chandra* data are not of sufficient quality to facilitate deprojection in small wedges to conclusively determine their nature. Given the arcsecond scale of these features, *XMM-Newton* does not have the spatial resolution to allow a useful deprojection.

3.2. Spectral Deprojection

We deprojected the temperature and density profiles of the gas in four different regions using the onion-peeling technique implemented in the model *project* of XSPEC12. These regions are an azimuthally symmetric region centered on the active nucleus (Region 1), a 30° wedge to the north of the nucleus extending to the surface brightness discontinuity (Region 2), a 30° wedge to the northeast of the nucleus in the opposite direction to the ram-pressure stripped tail (Region 3), and a 100° sector to the southwest (Region 4 - the ram-pressure stripped tail). Region 1 represents the average, azimuthally symmetric region of gas in the central 10 kpc. Region 2 corresponds to the gas interior to the surface brightness

discontinuity to the north of the nucleus. Region 3 lies along the direction of infall of NGC 4472 into the Virgo cluster gas. Region 4 traces the ram pressure stripped tail to the southwest. The positions of Regions 2 through 4 are shown in Figure 4.

We used a specifically tailored background dataset for the *XMM-Newton* deprojections created from other *XMM-Newton* observations near NGC 4472 with all point sources removed and reprojected on the sky with the appropriate instrument roll. We also deprojected the *Chandra* data in all regions that overlapped the *XMM-Newton* FOV as a consistency check. The nominal blank sky background was used for the *Chandra*/ACIS deprojection. We also evaluated the deprojections of the data from both observatories using a local background. The results are insensitive to the choice in background since the surface brightness of the emission from the NGC 4472 gas is significantly larger than that of the background. All three instruments (PN, MOS1, and MOS2) were used for the *XMM-Newton* spectral deprojections. The differences between the thermodynamic gas parameters measured with *XMM-Newton* and *Chandra* were insignificant (shown in Figure 7)

We initially fit the spectra using the APEC spectral model with the abundance as a free parameter; however, it was clear from the high quality spectra that the abundances of O, Fe, Mg, and Si did not scale in a linear fashion. We therefore used the VAPEC model in all spectral fits with the abundances of these elements allowed to vary freely. For the temperatures and densities determined via spectral fitting shown in Figure 7, the best fit abundances and uncertainties are tabulated in Table 1. These abundances are consistent with those reported by Humphrey & Buote (2006). In each shell, a single temperature VAPEC model with Galactic absorption was assumed. The temperatures in each shell were allowed to vary freely. The abundances of O, Fe, and Si were tied together across the shells, but allowed to vary independently. There is some evidence for complex spatial variation of the Fe abundance. All other elemental abundances were fixed at half the Solar value.

The deprojected hydrogen (n_H) densities and gas temperatures as a function of radius for the four regions are shown in Figures 7 through 10, respectively. The density profile from scales of ~ 100 pc (about $1''$) to ~ 30 kpc is remarkably smooth and monotonically decreasing. There are a few places where the density jumps up, but these are typically in the last bin of the deprojection where the technique will typically overpredict the density. The *Chandra* and *XMM-Newton* density deprojections track each other remarkably well where they overlap. We note that the density and pressure profiles in Figure 6 of Biller *et al.* (2004) were deprojected incorrectly and are incorrect. The pressure and density are significantly below the correct values (shown in Figure 7) at large radii. There is more variance in the data points in the temperature profiles than in the surface brightness or density profiles, but the central 1 kpc has a temperature of ~ 0.8 keV. The gas temperature increases to ~ 1.2 keV

at 30 kpc from the nucleus. Some of the apparent variance in gas temperature is probably related to the onion-peeling technique, but given the complex, non-azimuthally symmetric, temperature structure in the temperature maps above, some of the variance is also likely related to multi-phase structure in the gas that is simply not accounted for in the *project* model (i.e. it assumed that each shell is isothermal).

4. Interpretation

We find four previously undetected features in the hot gas in NGC 4472 using the deep *XMM-Newton* observation in combination with archival *Chandra* data. First, two sets of cool filaments extend ~ 25 kpc to the northeast and southwest of the active nucleus. One of these cool filaments is coincident with a sharp surface brightness discontinuity seen with *Chandra* (Biller *et al.* 2004). Second, we also report multiple surface brightness discontinuities in the *Chandra* data in the central ~ 5 kpc. Third, we find that the surface brightness discontinuity ~ 20 kpc north of the nucleus seen in the *Chandra* data extends much further east and west than previously observed. Finally, we detect a large-scale gas halo in which NGC 4472 is embedded, and characterize the previously reported ram-pressure stripped halo. *Chandra* and *XMM-Newton* have observed a large number of early-type systems in which the gas has been disturbed both by nuclear activity and by merging. It is likely that both processes play a role in creating the observed appearance of the gas in NGC 4472. We discuss the possible origin of these features and implications for the dynamical evolution of the group gas.

4.1. Contact Discontinuity

The surface brightness discontinuity in the gas (shown with the white arrows in Figure 1) extends more than $9'$ (~ 45 kpc) and has an irregular shape. There are at least two explanations for the surface brightness discontinuity 20-30 kpc to the north of the nucleus and the tail in the opposite direction: ram-pressure stripping and sloshing. The more likely scenario is that these features are the result of ram-pressure stripping of the core of NGC 4472 by the gas in the Virgo cluster as NGC 4472 falls toward M87. In this scenario, the direction of the ram-pressure stripped tail (southwest) suggests that NGC 4472 is falling into the Virgo cluster to the northeast, not directly toward M87 to the north. Another possible scenario is that the discontinuity and the tail are the result of ‘sloshing’ - non-hydrostatic gas motions due to a recent merger (Markevitch *et al.* 2001). However, there are several strong arguments against the sloshing hypothesis. First, NGC 4472 would had to have undergone a recent (< 1 Gyr) merger with a roughly similar size galaxy to disturb the gas on scales

of ~ 100 kpc. There is no evidence for a recent merger either in the X-ray data or in the optical isophotes of the central galaxy. Second, sloshing typically results in the X-ray emitting gas forming a characteristic spiral morphology (Ascasibar & Markevitch 2006), which is seen in X-ray observations of NGC 7618 (Kraft *et al.* 2006; Machacek *et al.* 2010b), NGC 5846 (Machacek *et al.* 2010a), and many other nearby galaxies, groups, and clusters (see Markevitch & Vikhlinin (2007) for a complete review). The long, straight tail and leading surface brightness discontinuity seen in NGC 4472 are more similar to what is expected in classical ram-pressure stripping, as seen in M86 (Randall *et al.* 2008) and NGC 4552 (Machacek *et al.* 2006). Finally, as we show below, the gas inside the discontinuity appears to be greatly overpressurized relative to the external gas and suggests transonic or supersonic motions, whereas gas motions in the sloshing scenario are almost always found to be subsonic ($v_{\text{gas}} \ll c_s$).

The merger origin for the gas features is confirmed by the pressure jump across the discontinuity. The gas pressure interior to the discontinuity is determined from the temperature and density profiles above, and is $\sim 4.2 \times 10^{-12}$ dyn cm $^{-2}$ ($n_H = 10^{-3}$ cm $^{-3}$ and $k_B T = 1.2$ keV). To determine the gas pressure exterior to the discontinuity, we use two estimates. First, the ROSAT PSPC image of the Virgo cluster clearly shows enhanced diffuse emission between M87 and NGC 4472 (Böhringer *et al.* 1994). The density profile of the gas within ~ 250 kpc of M87 was measured by Nulsen & Böhringer (1995) from this data. If we extrapolate this fit to the distance of NGC 4472 (~ 1.35 Mpc), we would estimate an ambient density of $\sim 1.0 \times 10^{-4}$ cm $^{-3}$, assuming that the infall of NGC 4472 is entirely in the plane of the sky. This value is consistent with that used in Irwin & Sarazin (1996). However, the enhanced surface brightness between M87 and NGC 4472 seen in the RASS image of M87 suggests that the density profile flattens to the south and east of M87. As an alternative, we fit the spectrum in a rectangular region $380'' \times 228''$ in the *XMM-Newton* data and on the I3 chip of the *Chandra* data (with point sources removed). The surface brightness of the emission is roughly twice the level of the dark sky background in both cases. We fit a single temperature APEC model to the spectrum and find $k_B T = 1.6 \pm 0.2$ keV (*XMM-Newton*) and $k_B T = 2.8 \pm 1.0$ keV (*Chandra*). The density of the gas, $n_{\text{filament}} \sim 2.2 \times 10^{-4} (\ell_{500\text{kpc}})^{-1/2}$ cm $^{-3}$, where $\ell_{500\text{kpc}}$ is the assumed path length through the gas in units of 500 kpc. We speculate that the enhancement seen in the ROSAT mosaic of the Virgo cluster is in fact a collapsed filament into which NGC 4472 is falling.

We estimate the infall velocity of NGC 4472 into this filament using the formalism of Vikhlinin *et al.* (2001) and model the infall as a steady flow around a blunt object. We use the density and temperature of the external gas measured above to estimate the pressure in the free stream region. This estimate is only accurate to a factor of ~ 2 due to the uncertainty in the path length of the gas exterior to the discontinuity. Note that the gas

density is unlikely to be much smaller than this since $n_H \sim \ell_{500kpc}$. Dropping the density (and pressure) by half would require the cylinder to have a diameter of 125 kpc, roughly the size of the *XMM-Newton* FOV at the distance of NGC 4472. Such a small linear size and volume would imply a noticeable gradient in the surface brightness across the *XMM-Newton* FOV, which is not observed. For $n_{\text{filament}} \sim 2.2 \times 10^{-4} \text{ cm}^{-3}$, the pressure of the gas exterior to the discontinuity is $2.2 \times 10^{-12} \text{ dyn cm}^{-2}$. We use the pressure just inside the discontinuity ($\sim 5 \times 10^{-12} \text{ dyn cm}^{-2}$) from Region 3 (the wedge to the northeast of the nucleus) as an estimate of the pressure at the stagnation point. We estimate the infall velocity to be Mach 1.1 or $\sim 950 \text{ km s}^{-1}$. For the lower value of gas density ($1.0 \times 10^{-4} \text{ cm}^{-3}$) and the same gas temperature (2.8 keV), the infall velocity will be considerably larger ($M=1.75$ or 1500 km s^{-1}). Note that the difference in recessional velocity between NGC 4472 and M87 is only 310 km s^{-1} . The infall of NGC 4472 into the Virgo cluster must therefore be nearly in the plane of the sky.

The gas interior to the discontinuity is not isobaric (in the absence of projection effects). In particular, the pressure of the gas inside the discontinuity directly to the north of the nucleus (Region 2) is more than twice that of Region 3. If the pressure of Region 2 is used as the pressure of the stagnation point, the infall velocity is estimated to be between $1500\text{--}2200 \text{ km s}^{-1}$ (depending on the external density). The ram-pressure stripped tail strongly suggests that the infall is to the northeast, not the north, so the higher pressure jump across the discontinuity to the north suggests that additional dynamical effects are important in shaping the observed morphology of the gas and/or there is significant structure in the gas along the line of sight.

There are several interesting conclusions that can be drawn from this result. First, we see no evidence of a bow shock being driven into the Virgo cluster gas/filament. For a Mach 1.5 shock, the density compression is a factor of 1.7 and the temperature increase is a factor of 1.5 just across the shock. The emissivity of the gas in this shell would be ~ 2.9 that of the ambient gas at a temperature of $\sim 2.4 \text{ keV}$. The distance between the bow shock and the contact discontinuity should be roughly 30% of the distance between the nucleus and the discontinuity, or 6 kpc (more than $1'$) (see appendix B of Vikhlinin *et al.* 2001, for a complete derivation). For low Mach numbers, this distance is a strong function of the Mach number, but for large Mach numbers it approaches an asymptotic value of ~ 0.15 . Such a shell, if present, should be easily visible in the *XMM-Newton* data. Either it is hidden by projection or we have significantly overestimated the infall velocity.

Second, the morphology of the contact discontinuity is very different than that seen in cluster mergers. In clusters, the contact discontinuity is typically seen as a continuous semi-circular arc with the vertex approximately centered on the peak of the gravitational

potential. For NGC 4472, there are several sharp bends in the surface brightness profile as one follows the discontinuity east of north. Contrast this with the discontinuity seen in the Abell 3667 merger (Vikhlinin *et al.* 2001) in which the discontinuity makes a smooth arc with a roughly constant radius of curvature. This suggests that the dynamics are more complex than simple gas stripping in NGC 4472, and that gas motions interior to the discontinuity are distorting this front.

Third, this simple analysis probably (significantly) overestimates the infall velocity of the NGC 4472 group into Virgo for the following reasons. First, cosmological cluster formation simulations demonstrate that massive sub-haloes can fall into filaments highly supersonically and retain a supersonic velocity after passing through the terminal shock of the filament (Skillman *et al.* 2008). Any gas that falls through the shock will be rapidly decelerated, but the gravitating sub-halo will proceed through the shock unhindered pulling its gaseous corona with it. This corona will be ram-pressure stripped by the gas in the filament. Second, the gas in the Virgo cluster filament into which NGC 4472 is falling is probably being accelerated toward the NGC 4472 group as it feels the group’s potential. That is, the dark halo of the NGC 4472 group is significantly larger than the distance between the nucleus and the contact discontinuity. A similar phenomenon has been reported in the Bullet cluster (Springel & Farrar 2007). The derived velocity represents the relative velocity between the NGC 4472 group and its infall into the Virgo cluster filament.

4.2. Internal Gas Dynamics

The temperature map (Figure 5) and surface brightness profile (Figure 6) of the gas interior to the contact discontinuity between the NGC 4472 group and Virgo cluster/filament gas indicate complex subsonic motions of the gas. The temperature map shows that the ~ 950 eV (the purple in Figure 5) gas is not symmetrically located around the nucleus, but displaced to the southeast. The cooler gas within ~ 1 kpc of the nucleus does not appear to have the same skew distribution relative to the nucleus. Additionally, the small surface brightness discontinuities are reminiscent of the sloshing cold fronts seen in the cores clusters of galaxies (ZuHone *et al.* 2009). There is a sharp change in the temperature and density across this jump, but the pressure jump is small. The various surface brightness discontinuities in the core of NGC 4472 represent contact discontinuities between slightly hotter and slightly cooler bits of gas that are circulating subsonically around the central gravitational potential. These features are typically visible only because of the n_H^2 dependence of the volume emissivity of the gas. The cooler gas is denser and therefore brighter. Finally, the hottest gas interior to the contact discontinuity with the Virgo cluster filament lies to the north of the nucleus, directly

behind the discontinuity (Figure 8). There is no evidence that NGC 4472 has undergone a recent merger and that these features are ‘sloshing’, but they are likely indicative of other subsonic gas motions, either due to the nuclear outbursts or to the dynamical process of merging with the Virgo cluster.

Hydrodynamic simulations of group/cluster mergers clearly suggest that while the dense gas in the cores of galaxies and groups is not stripped, the motion of outer gas that is stripped will induce circulation in the unstripped gas of the core (Heinz *et al.* 2003; Ascasibar & Markevitch 2006). This circulation will transport the low entropy gas from the core out to the region behind the contact discontinuity. Such a phenomenon has been proposed to explain the unusual morphology of the radio galaxy 3C 28 in the Abell 115 cluster (Forman *et al.* 2010). This radio galaxy lies in the dense cluster core of one of a pair of merging clusters and is a fairly typical FR II radio source with a narrow radio jet leading into a double lobed radio galaxy. Interestingly, the tails of both lobes are bent in the direction of infall (i.e. toward the contact discontinuity) of the merging core. If the tails were being swept back due to ram-pressure stripping by the external gas, they would be bent the opposite direction. It has been argued by Forman *et al.* (2010) that circulation of the gas in the dense core has pushed the tails of the lobes toward the contact discontinuity in the gas.

It is not clear, however, that the on-going merging/stripping has created the structures in the gas that we observe. The cool gas of the core appears displaced perpendicular to the direction of infall, not toward the contact discontinuity. Additionally, the appearance of the larger-scale (25 kpc) filamentary arms is not consistent with the ram-pressure stripping/merging scenario. These arms lie approximately along the axis of the infall of NGC 4472 as defined by the ram-pressure stripped tail (i.e. the northeast-southwest axis). It is hard to see how the filaments have remained long and straight given that the gas is likely rotational in this scenario, and why the filaments extend in both directions.

One other possibility for the origin of the filamentary arms is that the filaments are cool rims surrounding radio bubbles from a previous epoch of nuclear activity. These bubbles have risen buoyantly in the gaseous atmosphere and dragged the cool, low entropy material up from the center. Such features are commonly seen in the hot gas environments around radio galaxies, and have been observed in M87 (Forman *et al.* 2005), the Cen A Northern Middle radio lobe (Morganti *et al.* 1999), M84 (Finoguenov & Jones 2001), among many others. The radio bubbles are currently invisible (at least at GHz radio frequencies). A radio lobe may occupy the volume between each pair of the filaments. Note that in the cases of M87 (Owen *et al.* 2000) and Cen A (Kraft *et al.* 2009), bubbles from a previous epoch of nuclear activity appear to have reconnected to (or never disconnected from) the jet of the current outburst and are being re-energized. The old bubbles in NGC 4472 appear to

be truly dead and are not connected to the current epoch of nuclear activity. A deep, low frequency radio observation of NGC 4472 might resolve this by detecting these dead radio bubbles.

The terminal velocity for a buoyantly rising bubble is $\sim 0.4c_s$ (Churazov *et al.* 2001). If these filamentary arms are the result of a previous epoch of nuclear activity and are now rising buoyantly with this terminal velocity, they must be rising at $\sim 200 \text{ km s}^{-1}$, and their age is $\sim 10^8$ yrs. The total energy in these lobes is a relatively modest 2×10^{56} ergs. This is simply the total bubble enthalpy ($4pV$ per lobe) estimated using the exterior gas pressure. We assume that the lobe is a prolate spheroid with the long axes along each filament and the width (and depth) equal to the separation of the filaments in a given pair. Note that this estimate for the terminal velocity is applicable only if the size of the lobes is comparable to the distance between the lobes and the center of the potential. In our case, the lobes are smaller than this distance, so the buoyant velocity is somewhat less. A reasonable estimate for the age of these ghost lobes would then be several hundred million years.

A previous epoch of nuclear activity could also explain the distorted appearance of the contact discontinuity between the NGC 4472 gas and the Virgo cluster gas. In particular, the bend and elongation in the discontinuity could be the result of such gas motions. If the NGC 4472 gas is being driven out from the nucleus by a radio lobe, this would decrease the inferred infall velocity into M87 even further. That is, the $\sim 980 \text{ km s}^{-1}$ velocity measured at the discontinuity would not represent the infall velocity of NGC 4472 into M87, but would in fact be a combination of the infall of the group, the outward motions of the central gas due to the nuclear outburst, and the retrograde motion of the Virgo filament gas as it falls into the gravitational potential of the NGC 4472 group.

It is likely that both the buoyant rise of radio bubbles and circulation induced by the on-going merger play a role in the appearance of the structures we observe. The existing *Chandra* observation is not sufficiently deep to deproject the profiles in small wedges to measure the small temperature and density jumps predicted by the small surface brightness discontinuities, and *XMM-Newton* does not have sufficient spatial resolution to clearly resolve these features. It may be difficult to disentangle bubble from merger effects, but given the proximity, luminosity, and gas temperature of NGC 4472, a much deeper *Chandra* observation of this galaxy could provide a unique dataset for comparison with simulations to study subsonic and transonic (i.e. sound waves) dynamical phenomena.

4.3. Ram-Pressure Stripped Tail

The temperature and density of the gas in the ram-pressure stripped tail are shown in Figure 9. The tail extends beyond the field of view of the *XMM-Newton* observation, at least 50 kpc on the sky. Assuming that the tail lies in the plane of the sky, the total gas mass in the tail is $\sim 2 \times 10^9 M_{\odot}$ to a distance of ~ 40 kpc. The surface brightness, density, and pressure profiles of the gas in the tail are remarkably smooth suggesting that the stripping process is laminar and steady. Contrast this with the complex structures seen in the ram-pressure stripped tail of M86 (Randall *et al.* 2008). In M86, the tail is curved and bifurcated, and a large cloud of gas appears to have been completely separated from the main tail. Randall *et al.* (2008) argued that these features demonstrate that the tail is turbulent and that the gravitational potential is aspherical. Neither of these scenarios appear to be important for NGC 4472.

The ram-pressure stripped tail in NGC 4472 has some distinct differences with those seen in numerical simulations (Roediger & Brüggen 2008a,b) and *Chandra/XMM-Newton* observations of other Virgo cluster galaxies (Yoshida *et al.* 2002, 2004; Oosterloo & van Gorkom 2005; Sun & Vikhlinin 2005; Sun *et al.* 2006) and nearby merging groups (Kim *et al.* 2008). First, the opening angle of the tail is relatively wide (half-angle of $\sim 50^{\circ}$) with constant opening angle as a function of distance from the nucleus. In most of the other examples, the cross-section of the tail is roughly constant with distance from the central gas core. Additionally, the simulations of Roediger & Brüggen (2008a,b) show tails of ~ 40 kpc length for galaxies within 0.5-1.0 Mpc of the cluster center. The tail in NGC 4472 is considerably longer than those of the simulations, and the host galaxy is considerably further from the cluster center. Additionally, hydrodynamic simulations of ram-pressure stripping show a complex morphology that depends sensitively on the assumed gas viscosity (Roediger & Brüggen 2008a,b). A deep *Chandra* observation of the tail may be able to detect the small turbulent compressions and rarefactions predicted to be present in the tail.

NGC 4472 is known to have an unusually low X-ray luminosity relative to its total gravitating mass (Schindler *et al.* 1999). Based on the discussion in Section 4, it is clear why this might be the case. The ram-pressure stripped tail probably extends at least several hundred kpc (well beyond the field of view of *XMM-Newton*) and the group gas has been completely stripped by its infall into the filament. All that remains is the cool, dense core. The group gas has been left behind in a low density tail that may extend a degree or more behind the central galaxy.

5. Summary and Conclusions

We have presented results from a 100 ks *XMM-Newton* observation of the nearby massive early type galaxy NGC 4472. This observation has revealed a variety of structures in the gas indicative of a complex interplay of forces both internal and external to the group. In particular, we have shown that NGC 4472 is probably falling into a filament of the Virgo cluster, not directly into the cluster itself. There is a chain of galaxies and groups to the south and west of NGC 4472, including the massive early-type galaxies NGC 4365, NGC 4261, and perhaps NGC 4342, as well as all the associated smaller spiral and dwarf galaxies that may be part of this filament. A large-scale X-ray study of the hot gas along this chain of galaxies would provide detailed information about the structure and dynamics of filaments in clusters of galaxies. The proximity of the Virgo cluster makes such studies difficult because this filament spans several degrees on the sky.

We have also shown the presence of significant structure in the NGC 4472 group gas which is interior to the contact discontinuity. This structure is the result of both flow induced in the gas as part of the ram-pressure stripping process and multiple epochs of nuclear outbursts. We detect cold filamentary arms in the gas to the northeast and southwest that are likely cold, low entropy material that has been dredged up from the group center by an old radio outburst. Surface brightness discontinuities in the gas demonstrate that multi-phase gas has been mixed on scales of hundreds of parsecs.

6. Acknowledgments

This work was supported by NASA contract NAS8-03060, the *Chandra* X-ray Center, and the Smithsonian Astrophysical Observatory. MJH thanks the Royal Society for a research fellowship.

REFERENCES

- Anders, E. & Grevesse, N. 1989, *Geochimica and Cosmochimica*, **53**, 197.
- Ascasibar, Y. & Markevitch, M. 2006, *ApJ*, **650**, 120.
- Billier, B., Jones, C., Forman, W. R., Kraft, R. P., & Enßlin, T. 2004, *Ap. J.*, **613**, 238.
- Blakeslee, J. P. *et al.* 2009, astro-ph 0901.1138.
- Böhringer, H., Briel, U. G., Schwarz, R. A., Voges, W., Hartner, G., Trmper, J. 1994, *Nature*, **368**, 828.
- Churazov, E., Brggen, M., Kaiser, C. R., Bhringer, H., Forman, W. 2001, *ApJ*, **554**, 261.
- Churazov, E., Sunyaev, R., Forman, W., & Böhringer, H. 2002, *MNRAS*, **332**, 729.
- Côté, P., McLaughlin, D. E., Cohen, J. G., Blakeslee, J. P. 2003, *ApJ*, **591**, 850.
- Croton, D. J. *et al.* 2006, *MNRAS*, **365**, 11.
- David, L. P., *et al.* 2009, *ApJ*, submitted.
- Dickey, J. M., & Lockman, F. J. 1990, *ARA&A*, **28**, 215.
- Fabian, A. C., Sanders, J. S., Allen, S. W., Crawford, C. S, Iwasawa, K., Johnstone, R. M., Schmidt, R. W., & Taylor, G. B. 2003, *MNRAS*, **344**, L43.
- Finoguenov, A. & Jones, C. 2001, *ApJ*, **547**, L107.
- Forman, W. R., Jones, C., & Tucker, W. 1985, *ApJ*, **293**, 102.
- Forman, W. R., Jones, C., David, L., Franx, M., Makashima, K, & Ohashi, T. 1993, *ApJ*, **418**, L55.
- Forman, W. R., *et al.* 2005, *ApJ*, **635**, 894.
- Forman, W. R., in preparation.
- Heinz, S., Churazov, E., Forman, W. R., Jones, C., & Briel, U. 2003, *MNRAS*, **346**, 13.
- Humphrey, P., & Buote, D. 2006, *ApJ*, **639**, 136.
- Humphrey, Philip J., Buote, David A., Brighenti, Fabrizio, Gebhardt, Karl, & Mathews, William G. 2009, *ApJ*, **703**, 1257.

- Irwin, J. A., & Sarazin, C. L. 1996, ApJ, **471**, 683.
- Kim, D.-W., Kim, E., Fabbiano, G., & Trinchieri, G. 2008, ApJ, **688**, 931.
- Kraft, R. P., Jones, C., Nulsen, P. E. J., & Hardcastle, M. J. 2006, ApJ, **640**, 762.
- Kraft, R. P., *et al.* 2009, ApJ, **698**, 2036.
- Lowenstein, M., & Davis, D. S. 2010, ApJ, **716**, 384.
- Machacek, M., Nulsen, P. E. J., Jones, C., & Forman, W. R. 2006, ApJ, **648**, 947.
- Machacek, M. *et al.* 2010, ApJ, submitted.
- Machacek, M. *et al.* 2010, ApJ, in preparation.
- Markevitch, M., Vikhlinin, A., & Mazzotta, P. 2001, ApJ, **562**, L153.
- Markevitch, M., Gonzalez, A. H., David, L. P., Vikhlinin, A., Murray, S., Forman, W. R., Jones, C., & Tucker, W. 2002, ApJ, **567**, 27.
- Markevitch, M., Gonzalez, A. H., Clowe, D., Vikhlinin, A., Forman, W. R., Jones, C., Murray, S., & Tucker, W. 2004, ApJ, **606**, 819.
- Markevitch, M., & Vikhlinin, A. 2007, Phys. Rep., 443, 1.
- Morganti, R., Killeen, N. E. B., Ekers, R. D., Oosterloo, T. A. 1999, MNRAS, **307**, 750.
- Nulsen, P. E. J., & Böhringer, H. 1995, MNRAS, **274**, 1093.
- Oosterloo, T., & van Gorkom, J. 2005, A.& A., **437**, L19.
- Owen, F. N., Eilek, J. A., & Kassim, N. E. 2000, ApJ, **543**, 611.
- Randall, S., Nulsen, P. E. J., Forman, W. R., Jones, C., Machacek, M., Murray, S. S., & Maughan, B. 2008, ApJ, **688**, 288.
- Roediger, E., & Brüggen, M 2008, MNRAS, **388**, L89.
- Roediger, E., & Brüggen, M 2008, MNRAS, **388**, 465.
- Schindler, S., Bingelli, B., & Böhringer, H. 1999, A. & A., **343**, 420.
- Skillman, S. W., O’Shea, B. W., Hallman, E. J., Burns, J. O. & Norman, M. L. 2008, ApJ, **689**, 1063.

- Sun, M., & Vikhlinin, A. 2005, ApJ, **621**, 718.
- Sun, M., Jones, C., Forman, W., Nulsen, P. E. J., Donahue, M., & Voit, M. G. 2006, ApJ, **637**, L81.
- Springel, V. & Farrar, G. R. 2007, MNRAS, **380**, 911.
- Tonry, J. L., Dressler, A., Blakeslee, J. P., Ajhar, E. A., Fletcher, A. B., Luppino, G. A., Metzger, M. R., & Moore, C. B. 2001, ApJ, **546**, 681.
- Vikhlinin, A., Markevitch, M., & Murray, S. S. 2001, ApJ, **551**, 160.
- Werner, N., Zhuravleva, I., Churazov, E., Simionescu, A., Allen, S. W., Forman, W., Jones, C., & Kaastra, J. S. 2009, MNRAS, **398**, 23.
- Yoshida, M. *et al.* 2002, ApJ, **567**, 118.
- Yoshida, M. *et al.* 2004, AJ, **127**, 90.
- ZuHone, J., Markevitch, M., & Johnson, R. 2009, astro-ph 0912.0237.

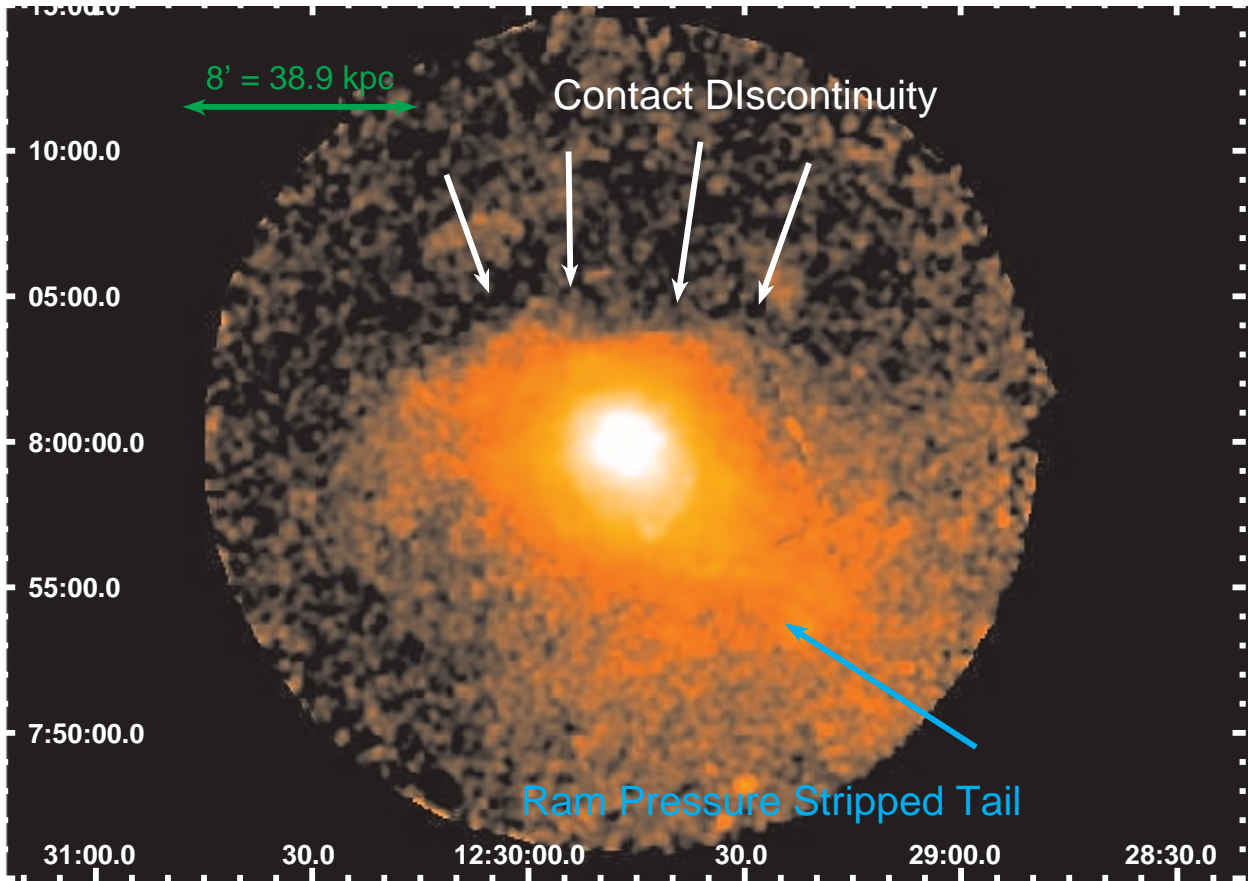


Fig. 1.— Exposure corrected, Gaussian smoothed ($\sigma=15''$) *XMM-Newton* image (MOS1+2 coadded) of NGC 4472 in the 0.5-2.0 keV band with point sources removed.

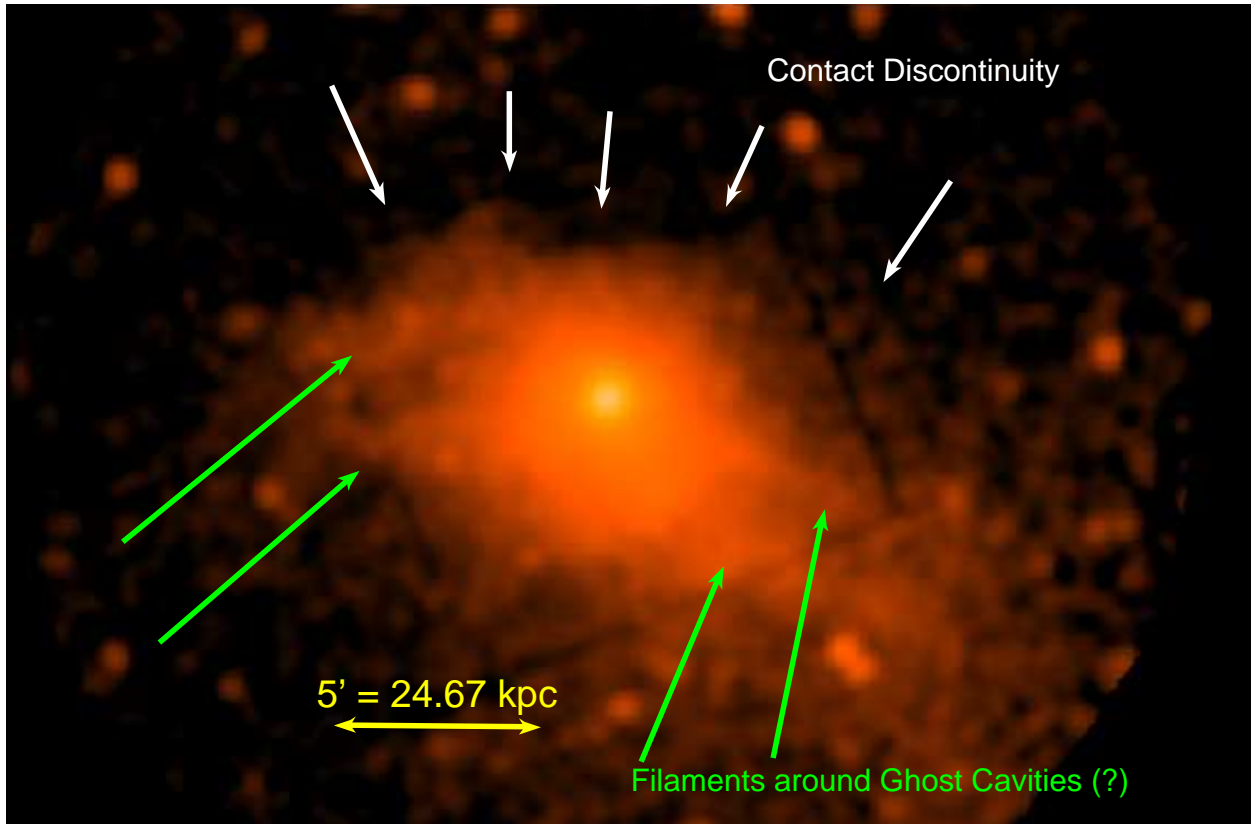


Fig. 2.— Exposure corrected, Gaussian smoothed ($\sigma=15''$) *XMM-Newton* image of NGC 4472 in the 0.5-1.0 keV band. The green arrows denote the positions of the four filaments possibly associated with ghost cavities. The white arrows denote the approximate position of the contact discontinuity between NGC 4472 and the Virgo cluster gas.

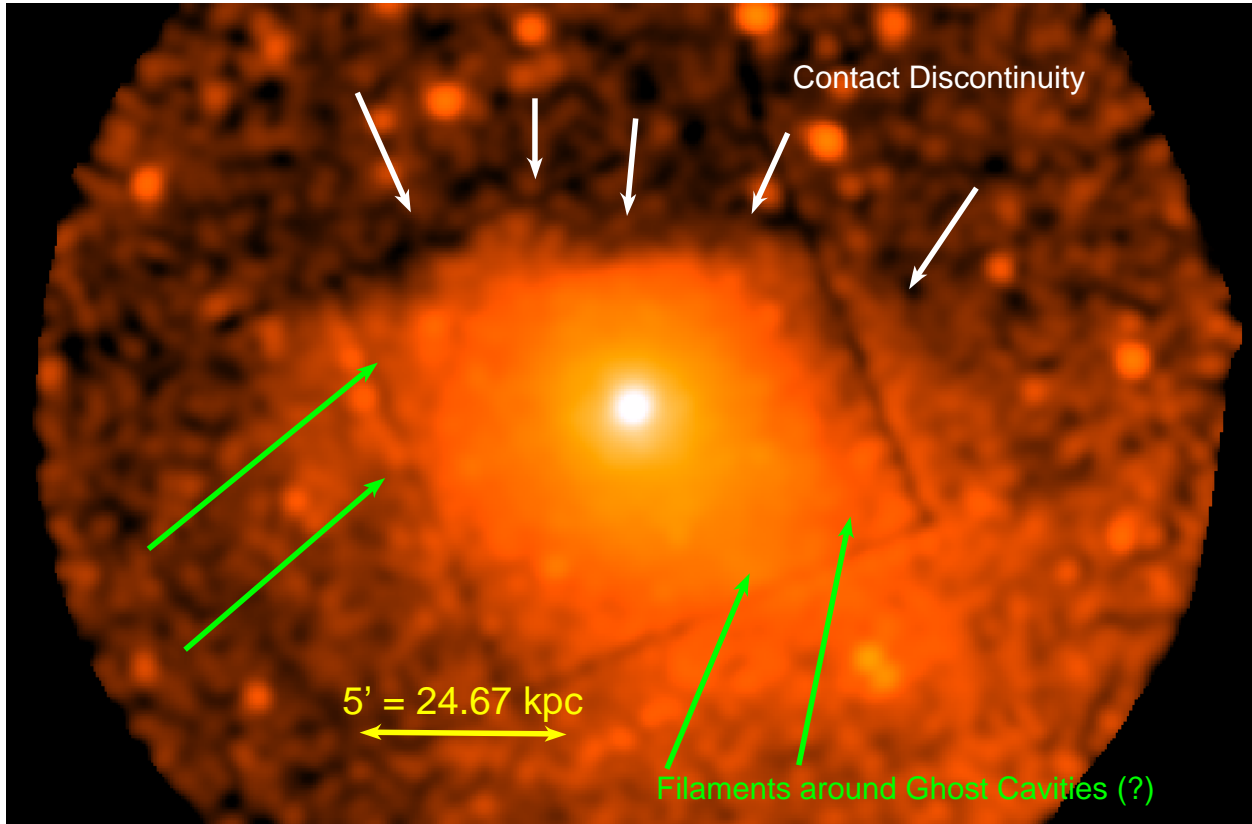


Fig. 3.— Exposure corrected, Gaussian smoothed ($\sigma=15''$) *XMM-Newton* image of NGC 4472 in the 1.0-1.5 keV band. The green arrows denote the positions of the four filaments possibly associated with ghost cavities seen in the softer band (Figure 2 but not in the harder band image). The white arrows denote the approximate position of the contact discontinuity between NGC 4472 and the Virgo cluster gas.

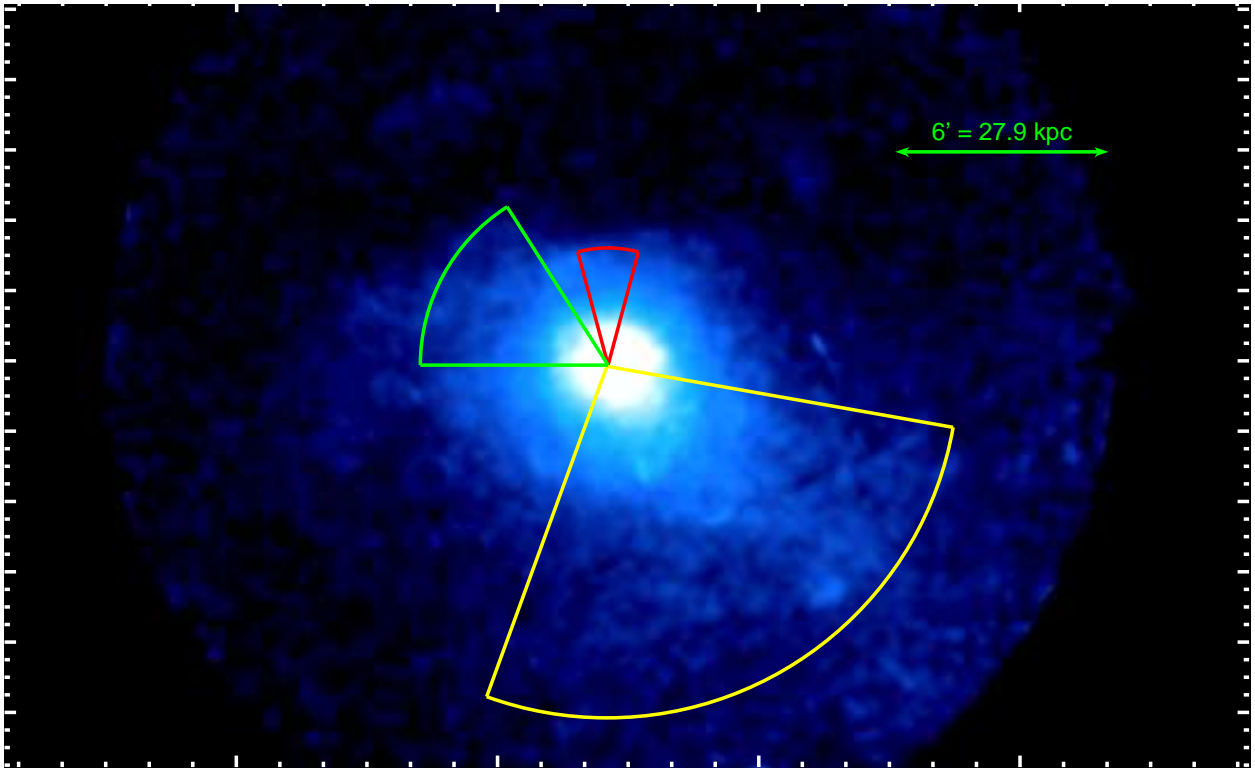


Fig. 4.— Exposure corrected, adaptively smoothed ($\sigma=7.5''$) *XMM-Newton* MOS1+2 image of NGC 4472 in the 0.5-2.0 keV band. The red, green, and yellow sectors correspond to Regions 2, 3, and 4 respectively. Region 1 (not shown in this figure) is a $2'$ radius circular region centered on the nucleus as described in the text.

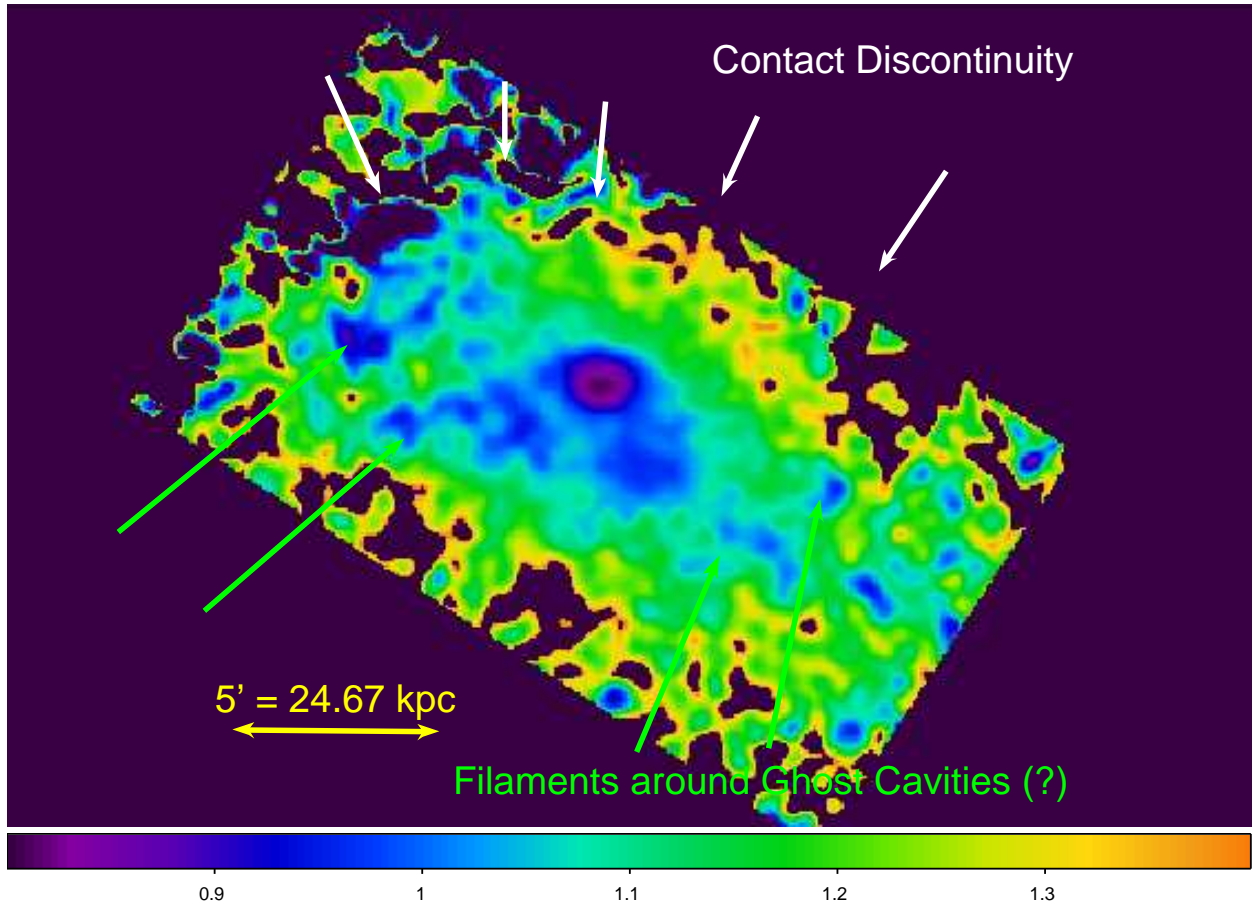


Fig. 5.— Temperature map of the NGC 4472 gas. The dense gas core is the purple at the center of the galaxy. The cool arms to the east and the southwest are shown as the dark blue and denoted by the green arrows - these cool filaments correspond to the surface brightness enhancements clearly visible in Figure 2. The white arrows denote the position of the surface brightness discontinuity - the contact discontinuity between the NGC 4472 gas and the Virgo cluster gas.

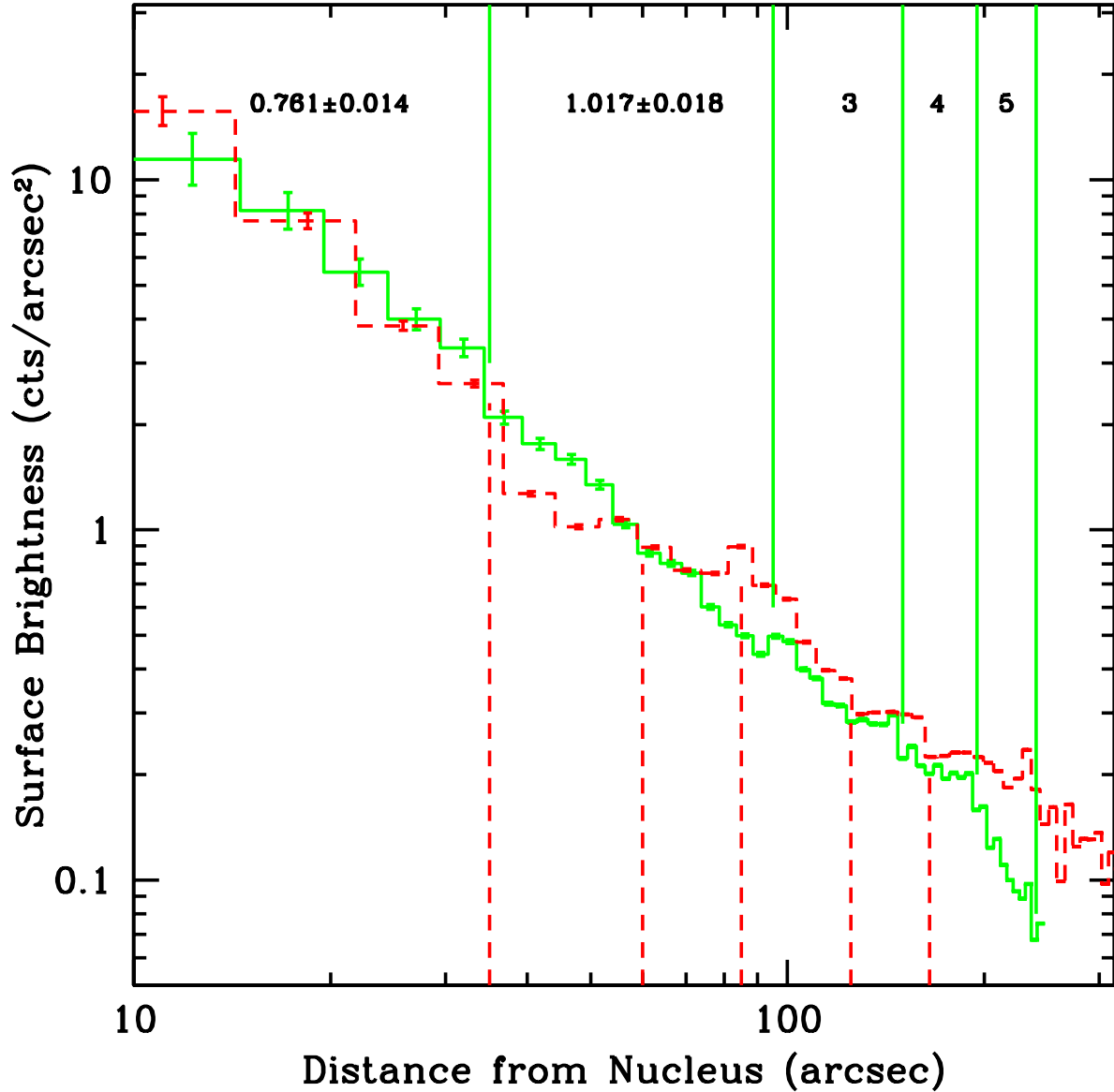


Fig. 6.— Surface brightness profiles in two wedges (green - northwest, red - northeast) centered on the nucleus of NGC 4472 in the 0.5-2.0 keV band. The green and red vertical lines denote the approximate positions of surface brightness discontinuities. The temperatures of Regions 3, 4, and 5 are 1.227 ± 0.042 , 1.228 ± 0.080 , and 1.36 ± 0.13 keV respectively (all uncertainties at 90% confidence for one parameter of interest).

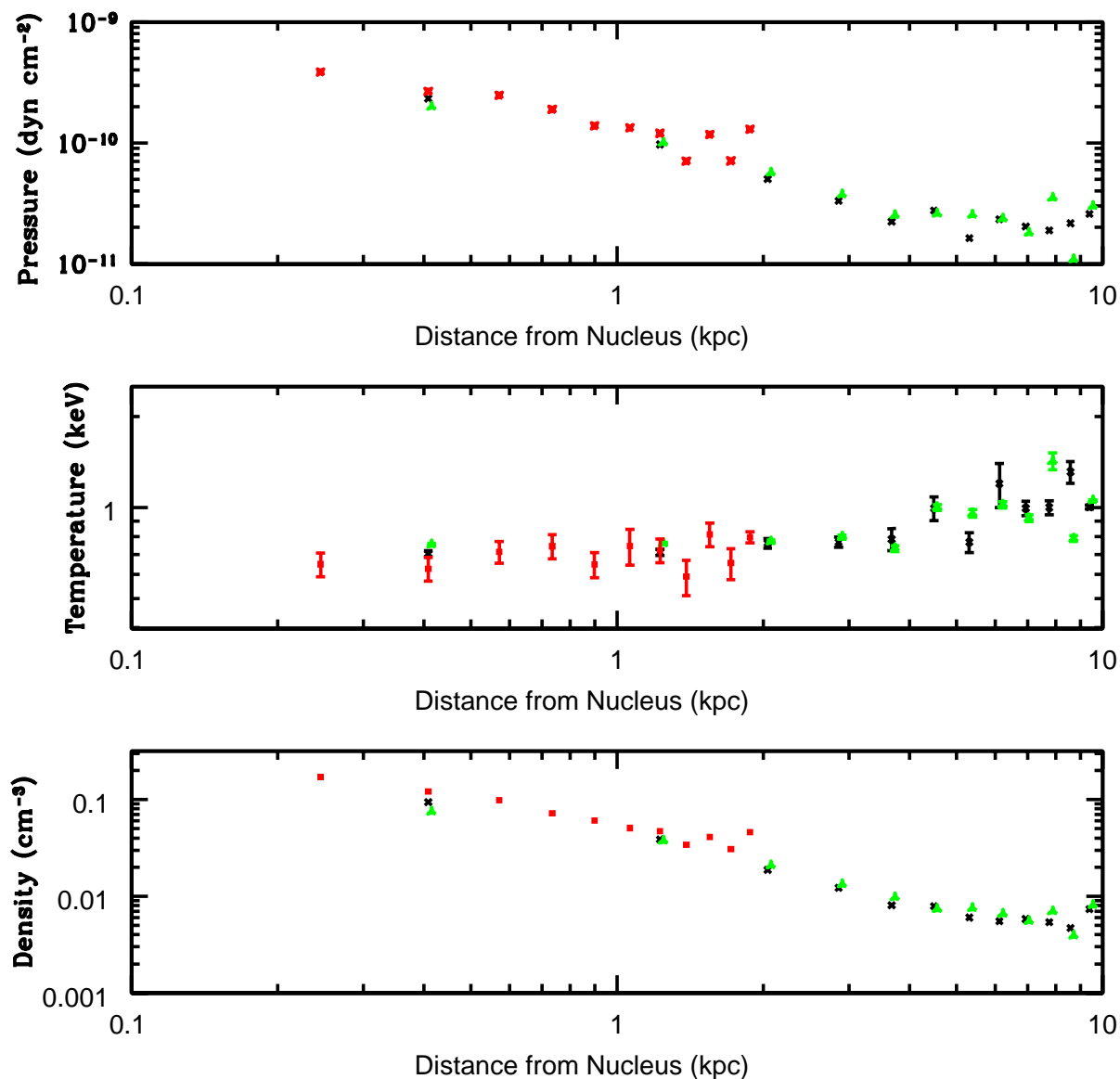


Fig. 7.— Deprojected density, temperature, and pressure profile of the gas in Region 1. The green and black points correspond to the profiles from the *XMM-Newton* and *Chandra* data, respectively. The deprojected profiles track each other remarkably well, indicative the systematic uncertainties related to the individual instruments are small. The small oscillation of the densities at the largest radii are artifacts of the deprojection technique and not significant. The red points are the *Chandra* deprojection of the thermodynamic parameters in smaller bins.

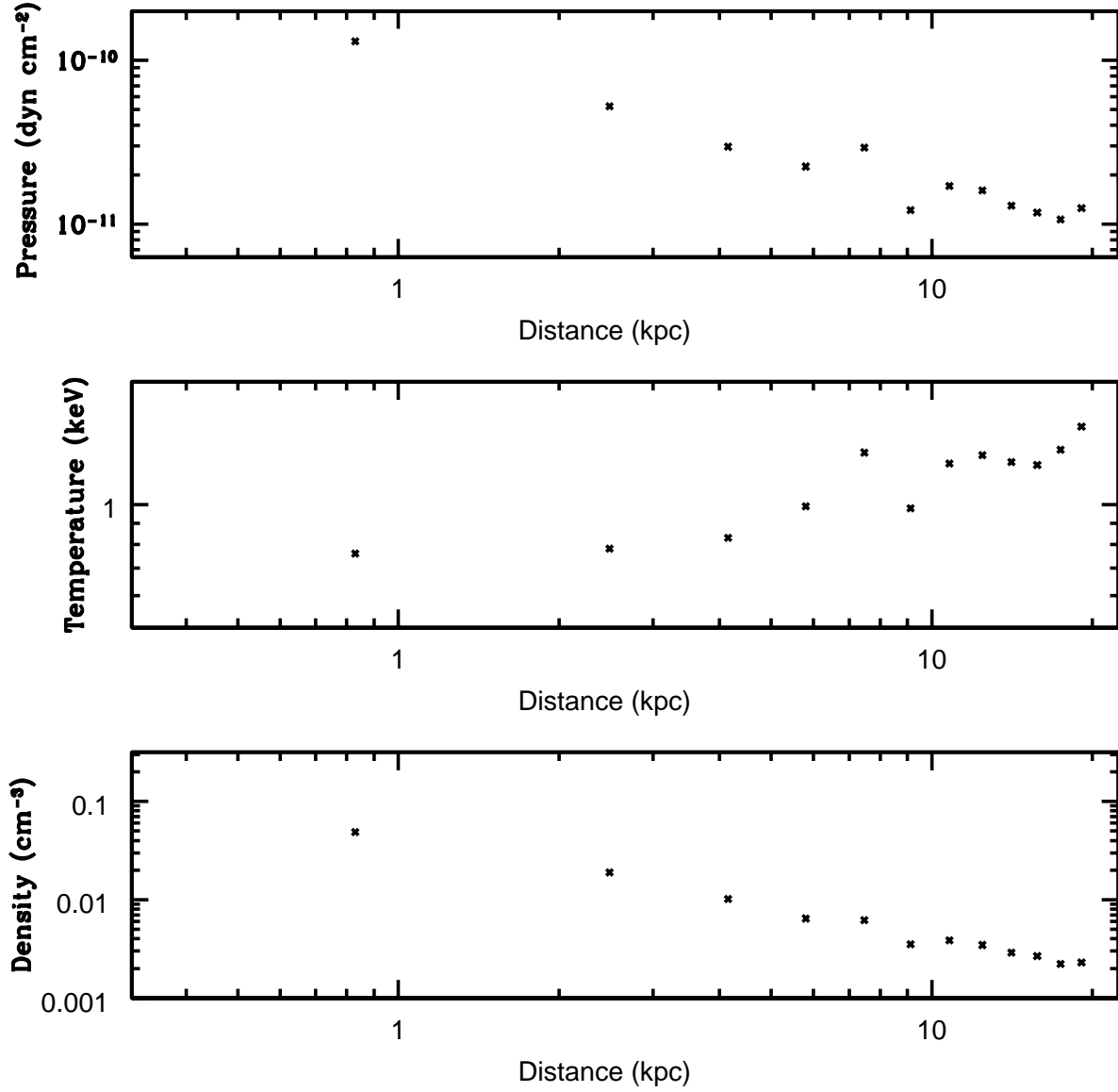


Fig. 8.— Deprojected density, temperature, and pressure profile of the gas in Region 2 (30° wedge to the north of the nucleus).

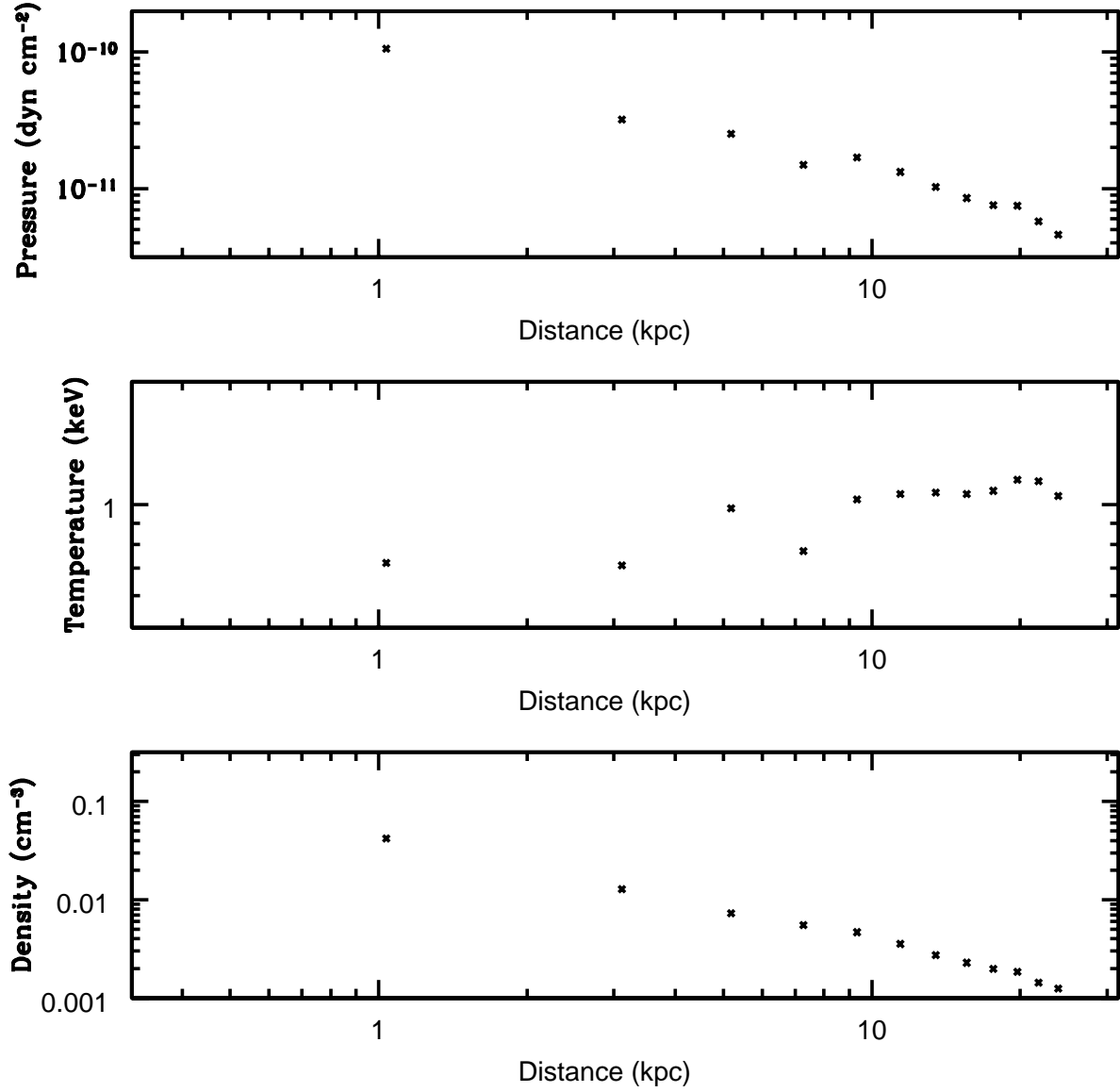


Fig. 9.— Deprojected density, temperature, and pressure profile of the gas in Region 3 (toward the direction of infall).

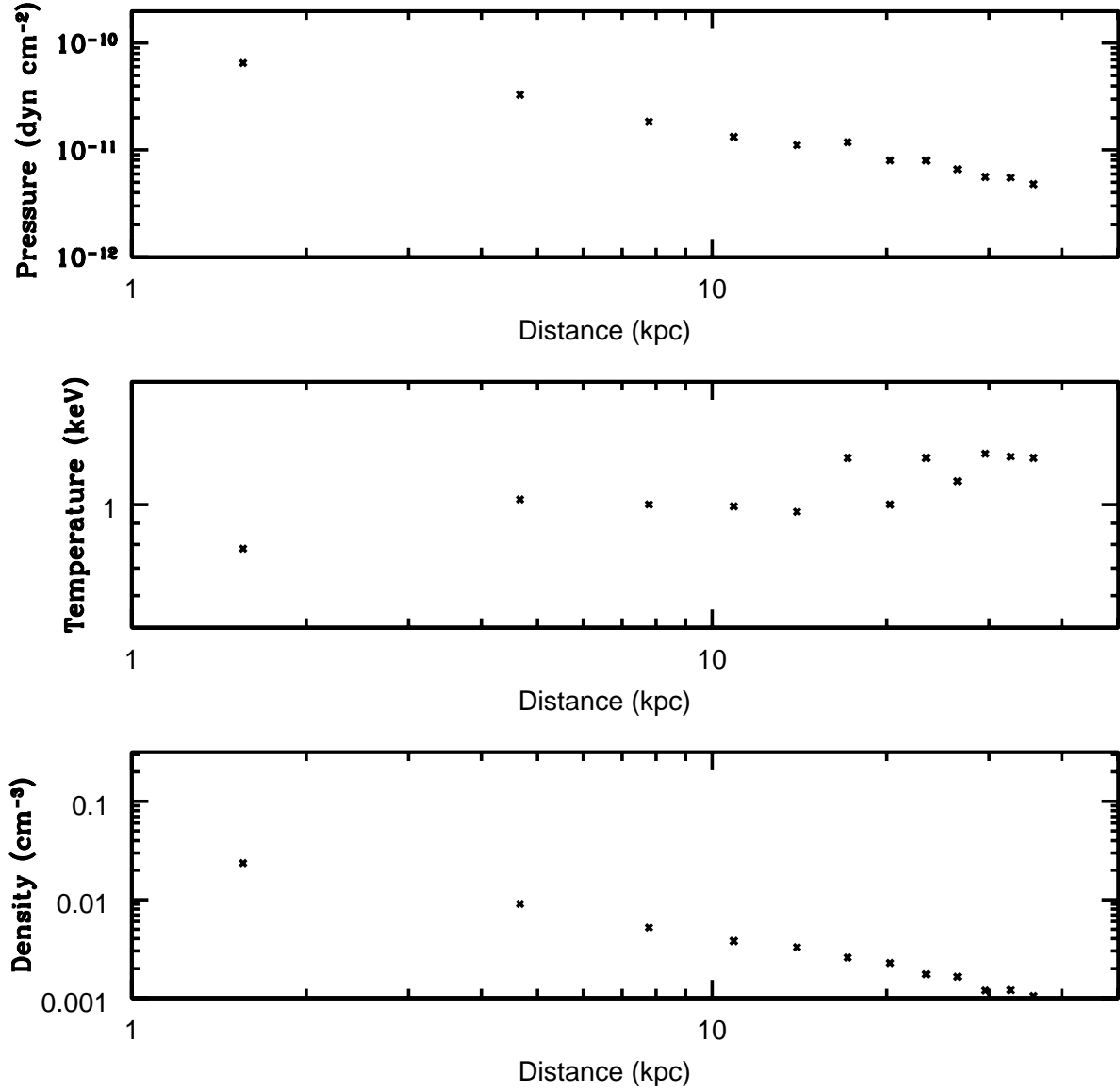


Fig. 10.— Deprojected density, temperature, and pressure profile of the gas in Region 4 (ram pressure stripped tail to the southwest of the nucleus).

Element	Value
O	0.34 ± 0.02
Si	1.04 ± 0.04
S	1.10 ± 0.08
Fe	0.63 ± 0.01

Table 1: Best fit elemental abundances in VAPEC model for azimuthally averaged profile (Region 1).